DOI:
10.1016/j.apt.2020.08.019

Document Version
Peer reviewed version

Low temperature Cu joining by in situ reduction-sintering of CuO nanoparticle for high power electronics

Yang Zuo[a,*], Sadie Carter-Searjeant[a], Mark Green[a], Liam Mills[b], Samjid H. Mannan[a]

[a]Department of Physics, King's College London, London, WC2R 2LS, UK

[b]The Manufacturing Technology Centre Ltd, Coventry, CV7 9JU, UK

Abstract:

Cu nanoparticles are promising interconnection material due to low cost and superior conductivity while they readily oxidize and need special processing and storing conditions. To solve these problems, a specific in situ reduction-sintering of CuO nanoparticles was developed and oxide free Cu submicron particles suitable for sintering were fabricated. The surfaces of the Cu submicron particles show no obvious oxide structure even after air sintering at 220 °C for 15 min and Cu-Cu joints with high shear strength of 22 MPa were produced. The oxide forms during longer bonding durations had a morphological evolution from stripe into grain and developed different layer structures on Cu particle surface. The micro-fracture mechanism of sintered Cu particles was analyzed and Cu particles were found to deform plastically while the surface oxide show obvious brittle fracture. Variation in shear strength with bonding time was analyzed and simulated based on contact area theory and the degradation of shear strength was correlated to the oxide formation. The proposed method produces similar shear strengths to Cu nanoparticle sintered joints but without the need for pressurized sintering or protective gas atmospheres.

Keywords: *Reduction-sintering; Oxidation; Nanoparticles; Fracture mechanism; Cu-Cu joining*

* Corresponding author: yang.zuo@kcl.ac.uk (Y. Zuo). +44 7422587334

1. Introduction

With the development of wide band gap semiconductors such as SiC and GaN, there is a requirement for lead-free interconnection materials which can survive at high temperatures (200 °C or higher) in order to support power electronics and other high temperature electronics applications [1]. Nanoparticle sintering is of interest because the sintering temperature can be brought down to low temperatures, typical of conventional soldering processes, even when the melting temperature of the bulk material is over 1000 K [2, 3]. Sintering of Cu nanoparticle is of particular interest due to copper's high thermal and electrical conductivity and strong electromigration resistance. However, high temperature or pressure assisted sintering with protective atmosphere is necessary to achieve acceptable sintering strength of Cu nanoparticles due to ease of oxidation, and this could increase the process complexity and damage some temperature sensitive devices [4, 5]. Kwon et al. [6] suppressed the oxidation of Cu nanoparticle during sintering by selective laser sintering, which possesses a faster sintering speed than a conventional furnace, while oxidation from environmental exposure during use is still inevitable and nanoparticle storage requires special conditions to prevent oxidation. Zuo et al. [7] coated a specific phosphating film on the surface of Cu nanoparticles and found that the Cu nanoparticles after treatment were free from oxidation at temperatures below 300 °C, However the consumption of the Cu nanoparticle during treatment was high and the dense phosphating film may hinder the coalescence between Cu nanoparticles.

To help address these issues, reduction sintering of CuO particle has been proposed. The reduction sintering process includes an additional reduction step of CuO particles followed by sintering of the reduced Cu particle. The total bonding time of CuO particle paste is normally much greater than that

of Cu particle paste, because sufficient reducing time is needed to completely transform CuO into Cu. Liu and Nishikawa [8] investigated a complex oxidation–reduction bonding process of Cu microparticles, which involves pre-heating samples at 130 °C for 5 min, heating at 300 °C for 20 min in air for microparticle oxidization, and holding at 300 °C for 40 min while introducing reducing formic acid atmosphere into the oven chamber. Gao et al. [9] further shortened the bonding time of this approach from 65 min to 35 min by pre-oxidizing the Cu microparticle at 300 °C for 8 min, but the total processing time is still non-ideal. Ogura et al. [10] replaced the complex reducing gas system by using the reducing solvent polyethylene glycol and found the reduction temperature 300 °C required for CuO nanoparticles is much higher than that for Ag_2O nanoparticles (150 °C) with the same reducing agent. In order to bring the bonding temperature of CuO particles down to an acceptable value for manufacturing (below 300°C), the reduction temperature should be as low as possible. A reducing organic solvent appears to be more promising than reducing gas due to its ease of manufacturing, but most typically used solvents will completely decompose or evaporate before reaching the reduction temperature. Therefore, the choice of reducing solvent for CuO reduction bonding is limited and the oxidation mechanism of the Cu particles during sintering and its impact on sintering strength requires more research.

In this study a specific in situ reduction-sintering of CuO nanoparticles was developed to fabricate strong Cu-Cu bonding without special processing conditions. The growth behavior and morphological evolution of oxide during sintering were detailed and the effect of oxide on the sintering strength of Cu particles was investigated. The micro-fracture mechanism of sintered Cu particles was also studied.

2. Materials and methods

CuO nanoparticles with mean diameter of 100 nm purchased from Sigma-Aldrich were used in this study. The initial morphology is as shown in **Fig. 1**. Ascorbic acid and ethylene glycol were mixed as reducing agent I, glycerol and polyethylene glycol (PEG) were chosen as reducing agent II and III. The paste was composed by mixing CuO nanoparticle with reducing agent. The mass ratio of CuO to reducing agent was 2/8 except reducing agent I (15wt% of CuO, 15wt% of ascorbic acid and 70wt% of ethylene glycol). The reduction temperatures of CuO nanoparticle for each reducing solvent were evaluated by Differential Scanning Calorimetry (STARe DSC822e) at a heating rate of 20 K/min in air. The phase composition of reduced Cu particles before and after sintering was measured by X-ray diffraction (Stoe StadiP, X-ray radiation: Mo Kα1 (using 50kV and 30mA), 2θ scan range: 2.000° to 50.015°, 0.495°/5 s).

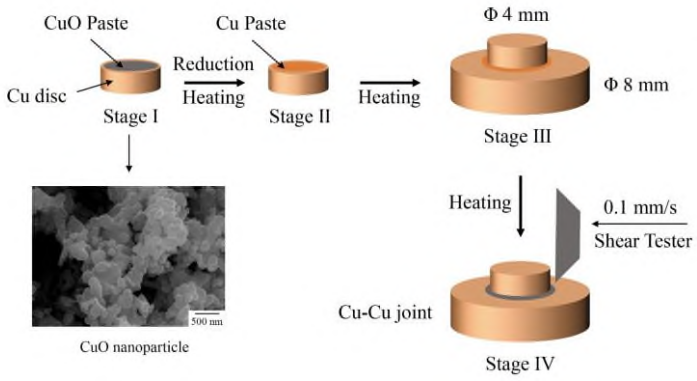

Fig. 1 SEM image of CuO nanoparticle and Schematic illustration of Cu-Cu joint in bonding experiment and shear test.

Cu discs of 4 mm diameter and 2mm thickness (small) and 8mm diameter and 3mm thickness (large) acted as component and substrate respectively. Prior to bonding, the discs were polished with emery paper (up to 800-grit), soaked briefly in diluted hydrochloric acid, rinsed in ethanol and dried. The paste was firstly printed on the surface of the small Cu disc (the height of the paste drop is 2 mm)

and then heated to the reducing temperature of the organic solvent for several minutes as shown schematically in **Fig. 1**. Following reduction, the smaller Cu disc with reduced Cu particles was forced face down on the top of larger Cu disc with placement pressure of 3 MPa for 1 minute to ensure good contact between the paste and the Cu discs. Next the assemblies were heated to 220 °C for 10 min, 15 min, 20 min, 40 min, 80 min and 240 min without pressure on a hot plate (Stuart SD160) in air in order to determine the effects of sintering time. The shear strengths of joints were assessed by means of a shear tester (Nordson Dage 4000+) at room temperature and the mean values of ultimate shear strengths of five specimens for each bonding condition were calculated and reported for comparison. The morphology of CuO nanoparticle and reduced Cu particle, fracture surface and cross section of joint specimen were observed by Field-emission scanning electron microscopy (Hitachi S4000) equipped with energy dispersive X-ray Spectroscopy (EDS) and Transmission electron microscope (JEOL JEM-1400), the EDS results are calculated from the mean values of three different area of sample for each condition. The particle size measurement was carried out with "ImageJ" software and three different images of sample for each condition were measured.

3. Results

Reducing agent I was ascorbic acid. Since an organic solvent is necessary to disperse the CuO nanoparticles and fabricate the paste, ethylene glycol was mixed with the ascorbic acid (powder) to make the reducing solutions. The paste mixed by ethylene glycol and CuO nanoparticles was tested by DSC as shown in **Fig. 2 (a)**. The result shows that there is no exothermic peak in the red curve, indicating that CuO nanoparticles cannot be reduced by ethylene glycol liquid alone. Next, ascorbic

acid was mixed with ethylene glycol and CuO nanoparticles. It can be concluded that the exothermic peak at 135 °C in the black curve shown in **Fig. 2 (a)** was caused by the reduction reaction between ascorbic acid and CuO nanoparticles [11]. The mean diameter of reduced Cu particle by ascorbic acid at 135 °C was 500 nm and the shape was spherical as shown in **Fig. 3 (a)**. However, the EDS results show the existence of carbon indicating the presence of organic residues after reduction, which would significantly hinder the coalescence between Cu particles during sintering. The organic residues may decompose at higher temperature while high sintering pressure is necessary to compress the particles for achieving dense sintering structure.

By comparing the difference between the curves of reducing agent II, glycerol and reducing agent III, PEG with and without CuO nanoparticles, the reducing temperature of the organic solvent is found by the position of the additional exothermic peak in the black curve. PEG had the highest reducing temperature of 320 °C and produced in the smallest reduced particle size of 300 nm. There was still some organic compound covering the reduced particles as shown in **Fig. 3 (b)** and the corresponding EDS results also show the existence of carbon. Meanwhile, an unacceptably high sintering temperature of over 320 °C is necessary to decompose these organic compounds. The reduction temperature of glycerol was 220 °C and reduction reactions began at just 200 °C. The reduced Cu particles have a larger mean size of 1 μm and a cleaner surface as shown in **Fig. 3 (c)**. Carbon was not detected on the reduced Cu particles which indicates that most of the organic compounds decomposed. Metal nanoparticles have been reported to grow through merging primary particles and organic ligands serve as stabilizers to prevent nanoparticle merging [12]. Love et al. [13] also reported that the organic shell can act as a physical or electrostatic barrier against aggregation of

nanoparticle. These results suggest that organic residues on particle surfaces can depress Cu particles growth by preventing them merging and result in a smaller particle size. Therefore, it can be concluded that glycerol is the optimal reducing agent for CuO nanoparticle with the mean size of reduced particle being 1 μm. The main reduction reaction of CuO by glycerol is given in eq. (1) while the oxidation products will vary according to the degree of oxidation [14, 15]:

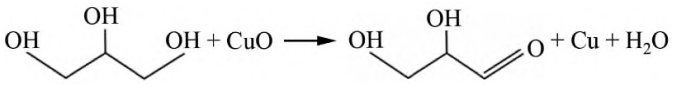

(1)

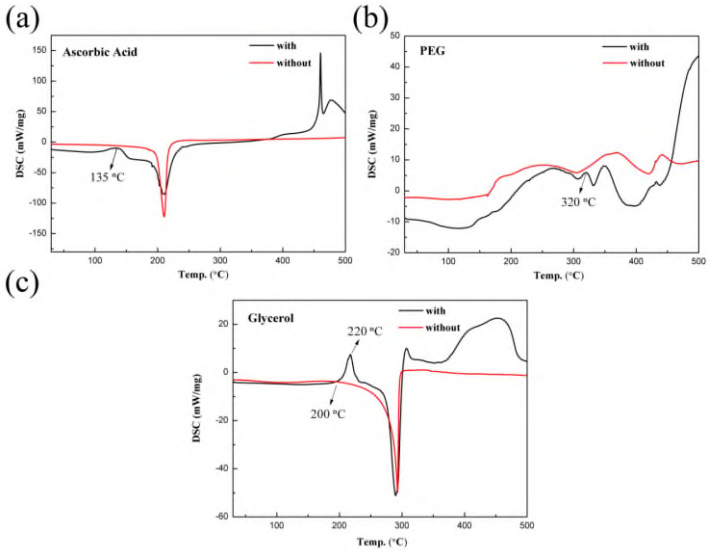

Fig. 2 Thermal analysis of (a) ethylene glycol and CuO nanoparticle with and without ascorbic acid, PEG (b) and glycerol (c) respectively with and without CuO nanoparticles.

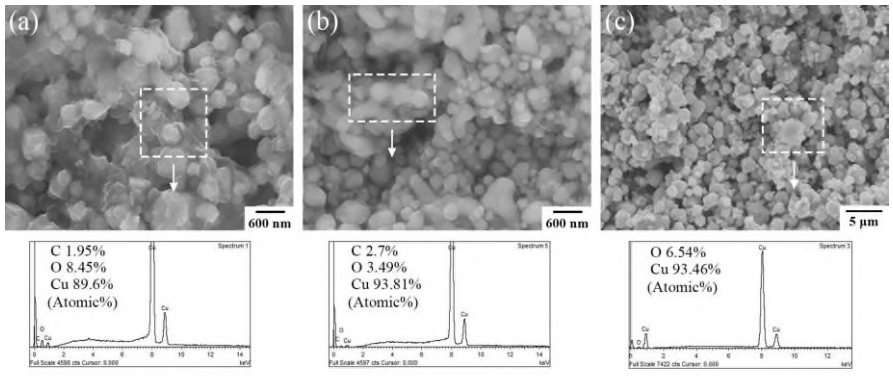

Fig. 3 Morphology and EDS results of reduced Cu particle by ascorbic acid at 135 °C (a), PEG at 320 °C (b) and glycerol at 220 °C (c).

Fig. 4 shows the morphology and size distribution of the reduced Cu particles by glycerol at 200 °C, 210 °C, 220 °C and 230 °C. The minimum required durations of the reduction step with different temperature were also measured (the counting begins after putting the small disc with printed paste on hot plate and ends when no reaction bubble forms). With increasing reduction temperature, the shape of the reduced particles remained spherical while the reduction time was greatly shortened from 6 min and 20 sec at 200 °C to 2 min and 12 sec at 230 °C. The reduced Cu particles at different temperatures shear similar mean diameter and size distribution. However, the water reaction byproduct will boil and fabricate bubbles in the paste during reduction. Higher reduction temperature will cause more violent reaction and severe paste splash which is negative to manufacturing. Meanwhile the Cu particle oxidizes easily at higher temperature negating the benefit of reduced reduction time. Higher temperature may also damage some sensitive electronics components and raise cost. Therefore, the 220 °C temperature has been determined as the most suitable reduction temperature of CuO nanoparticles by glycerol.

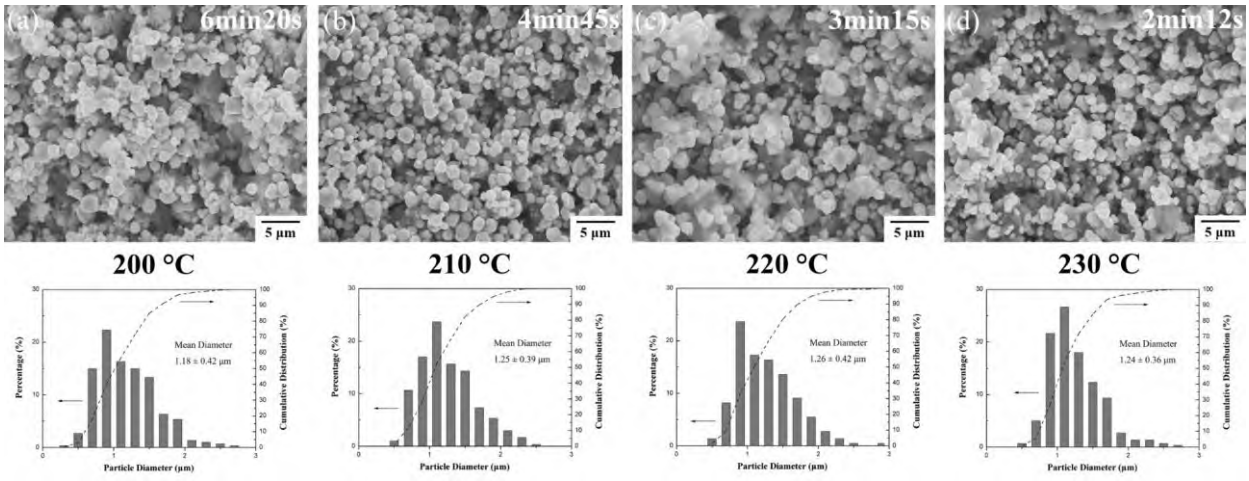

Fig. 4 Morphology and size distribution of reduced Cu particle by glycerol at 200°C (a), 210 °C (b), 220 °C (c) and 230 °C (d). Required reduction times are shown in figure.

In order to confirm the most suitable mass ratio between CuO nanoparticles and glycerol, the

phase composition of fracture surfaces of joints with differing concentrations of CuO in the paste was analyzed by X-ray diffraction (Mo radiation) as shown in **Fig. 5 (a)**. With low CuO content, only Cu peaks can be detected. However, when the mass ratio rises to 40%, obvious Cu_2O peaks began to appear. Since a higher concentration of CuO nanoparticles leads to more reduced Cu particles in the paste and a denser sintering structure, the mass ratio of 3.5:6.5 is most suitable.

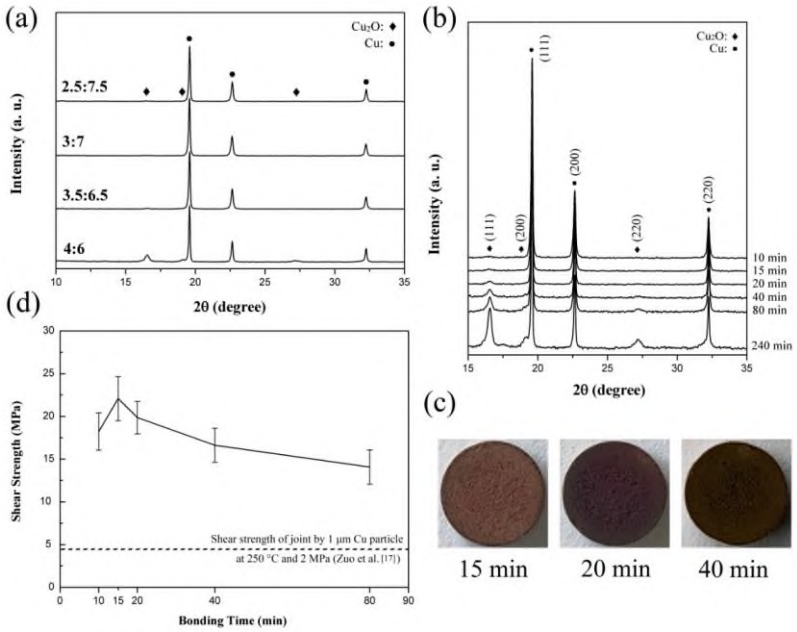

Fig. 5 XRD patterns (a) of fracture surfaces of joints with different mass ratios of CuO nanoparticle to glycerol, XRD patterns (b) and images (c) of fracture surfaces and shear strengths (d) of (3.5:6.5) joints for different bonding time.

Fig. 5 (b) shows the XRD patterns (Mo radiation) of fracture surfaces of (3.5:6.5) joints with different bonding times. When the bonding times were 10 min and 15 min, XRD patterns show obvious peaks of metallic Cu and the intensity of the Cu_2O peak was negligible. However, the corresponding EDS results of the 15 min joint (see Supplementary material **Fig. S1**) show an oxygen content of 11.59 % which indicates that the Cu particles were slightly oxidized. As time rose to 20 min, a Cu_2O peak corresponding to the crystal plane of (111) began to appear, and the color of Cu

sintered particles also changed from their natural orange into dark red due to the formation of Cu_2O as shown in **Fig. 5 (c)**. As time further rose to 40 min, another two Cu_2O peaks related to crystal planes of (200) and (220) were detected, while the strength of peaks was weak. The oxygen content also increased to 25.99 % (see Supplementary material **Fig. S2**) and the color of Cu sintered particles further changed to dark grey. The strength of these three Cu_2O peaks became stronger with further increasing time. However, even with 240 min bonding time, no obvious CuO peak was found. Yang et al. [16] reported similar results that only the Cu_2O formed on the surface of Cu powder at 200 °C and formation of CuO occurred at 300 °C. Therefore, it can be concluded that Cu_2O is the only oxidation product of Cu particles within 240 min of sintering at 220 °C.

From the point of view of manufacturing, Cu-Cu bonding should be performed at a reasonably low temperature and pressure with a time that is as short as possible. The joints for shear test were fabricated with bonding times between 10 min and 80 min. The shear strengths of joints using 3.5:6.5 paste are plotted in **Fig. 5 (d)** as a function of bonding time (error bars calculated by mean value ± one standard deviation of shear strengths). From this plot it is apparent that the shear strength of the joint increased firstly with increasing time and reached a peak of 22 MPa at 15 min even though a certain amount of oxygen already existed. Then it decreased as bonding time rose to 20 min where obvious Cu_2O began to appear according to the XRD results. These results indicate that the formation of Cu oxide structure is responsible for the degradation of joint shear strength. Zuo et al. [17] employed Cu microparticles with a size of 1 μm and non-reducing organic solvent to fabricate Cu-Cu joints, with the higher temperature of 250 °C and sintering pressure of 2 MPa. Under these conditions the reported joint strength is nearly five times lower than the best shear

strengths of the current (3.5:6.5) joints as shown in **Fig. 5 (d)**. Compared with traditional Cu nanoparticle sintering, the in situ reduction-sintering omits the heating step from room temperature where Cu oxidation usually appears. Meanwhile, the reduced Cu submicron particles have higher oxidation resistance than Cu nanoparticles can be quickly and directly sintered at the reduction temperature. These properties lead to the high shear strength of joint formed by this method.

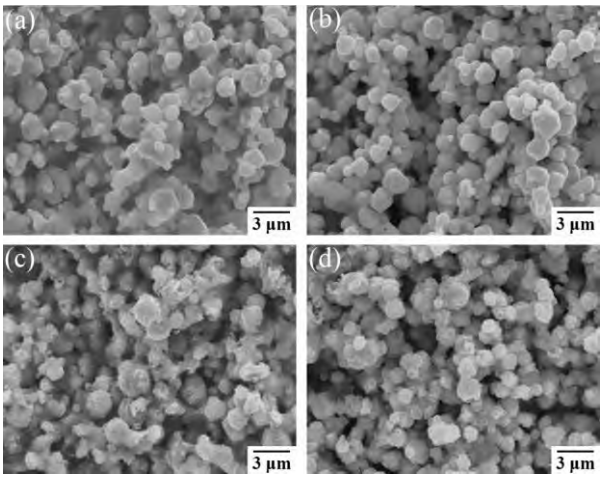

Fig. 6 SEM fracture surface images of joints for 15 min (a), 20 min (b), 40 min (c) and 80 min (d).

Fig. 6 shows SEM images of fracture surface of the (3.5:6.5) joint for different bonding times. The morphology of the fracture surface shows little change with increasing time while the surface of the Cu particle changed from smooth to rough due to the formed oxidation film. Meanwhile, Cu particles have deformed little and significant coalescence between particles was not found. It is also clear that the fracture mainly located at the interface between Cu particles. To investigate the effect of oxidation on the sintered structure, the 15 min joints with best strength and no obvious oxide were compared with the 40 min joints with clear oxide structure. SEM cross section images of representative joints after cutting and polishing are shown in **Fig. 7**. Both cross sections of 15 min and 40 min show a dense and porous structure and significant sintering coalescence between particles was found as shown in **Fig. 7 (b)** and **(d)**. The interfaces between Cu particles and disc also

show good bonding as shown in **Fig. 7 (c)** and **(f)** and the Cu particles have deformed due to interdiffusion with the substrate. However, by comparing the images of cross section of 15 min and 40 min, it is clear that an oxidation film has formed on surface of particles at 40 min as shown in **Fig. 7 (d)** and **(e)**, depressing further diffusion of Cu atoms and causing poor sintering strength, which is in good in agreement with shear test results. In order to prove the existence of the oxidation film, the sintered Cu particles with uneven surface in the 40 min joints cross section was polished and the oxide in only outer Cu particle was removed while the oxide in inner Cu particle remained as shown in **Fig. 7 (g)**. The relevant EDS results show that the oxygen content of the polished particle is much lower than that of unpolished one. Meanwhile, the oxygen content of cross sections of 15 min joint (8.01%, see Supplementary material **Fig. S3**) and 40 min joint (19.17%, see Supplementary material **Fig. S4**) were both lower than the values (11.59% and 25.99%) of the corresponding fracture surface, which indicates that the fracture tends to appear in the sintering areas with high oxidation.

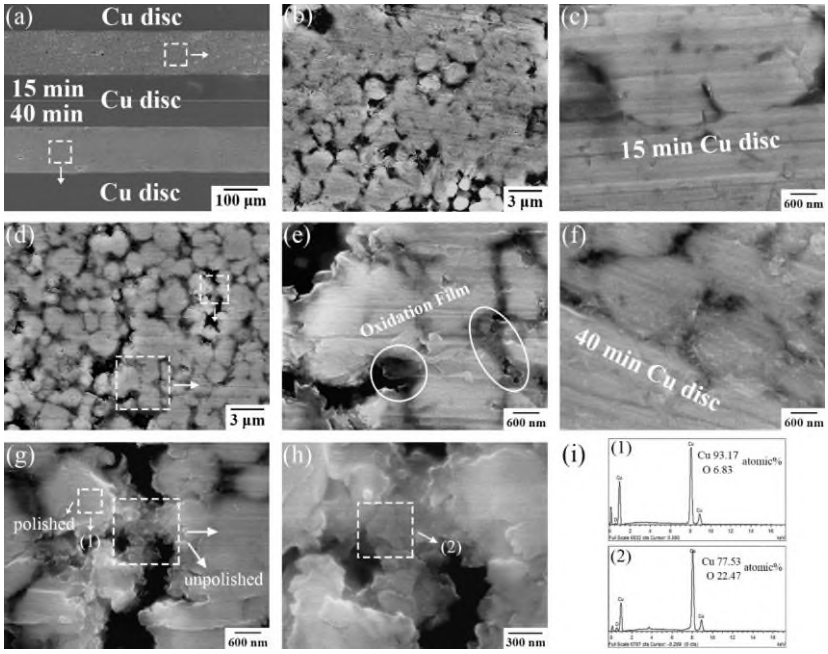

Fig. 7 SEM cross section images of joints bonded for 15 min (a, b, c) and 40 min (d, e, f, g, h), as well as corresponding EDS results (i).

4. Discussion

4.1 Growth behavior of cuprous oxide

The primary oxide formed on the surface of Cu micro/nano particle during low temperature sintering has been reported to be cuprous oxide (Cu_2O) and its formation plays a critical role in determining the shear strength of Cu-Cu joint [7, 8]. However, growth behavior and morphological evolution of Cu_2O during sintering still remain unclear and require further study. Cu_2O with cubic crystalline structure has been reported to grow epitaxially on the Cu surface. The sequence of oxidation reactions on a clean metal surface is generally accepted to be oxygen chemisorption, nucleation and growth of surface oxide, and bulk oxide growth. Before the onset of oxidation, a restructured Cu surface due to oxygen saturation has been proven to be important for formation of Cu_2O. Lee et al. [18] reported that the subsurface oxide-like structure was more easily produced on a Cu surface with pre-adsorbed oxygen atoms. The mechanism of nucleation and initial growth of oxide islands on a clean Cu surface has been proposed in terms of 'capture zone' theory [19], which claims that oxygen atoms diffuse on Cu surface and become incorporated into an oxide island when entering the surrounding capture zone. After oxide islands reach the saturation point of nucleation, they start to grow and coalesce to generate a thin layer of Cu_2O. Oxygen diffusion dominates initial growth of the oxide, and direct impingement of oxygen atoms onto islands is also likely to occur when island size becomes larger [20]. The formed Cu_2O layer prevents exposure of Cu to oxygen. Further oxidation of Cu occurs on both internal and external surfaces of the oxide layer and is a result of Cu atoms from the underlying Cu metal core diffusing outward through the oxide layer and oxygen atoms diffusing into the Cu core. Meanwhile, Hung et al. [21] reported that oxygen atoms are

absorbed into oxide layer surface and electrons penetrate into the layer by tunneling to establish equilibrium between Cu ions and oxygen ions, this process produces an electric field which provides an additional driving force for Cu ions move outward.

The surfaces of Cu particles for 15 min were very clean and show no obvious oxide structure as shown in **Fig. 8 (a)** and **(e)**, which matches the corresponding XRD results very well (presented in Section 3). The existence of oxygen detected by EDS can be attributed to oxygen chemisorption and nucleation of oxide islands, which are inevitable for air sintering at 220 °C. When bonding time is 20 min, oxide islands reached the saturation point of nucleation and started to grow and show an irregularly striped structure as shown in **Fig. 8 (b)**. They later coalesced together and produced a thin Cu_2O laminar layer termed Cu_2O layer I as shown in **Fig. 8 (c) and (j)**. Additionally new oxide islands formed and grew on the surface of some existing Cu_2O layers I to produce a multilayer structure. As time further rose to 40 min, oxide islands with a second morphology of Cu_2O grain began to appear and showed a spherical structure with a mean diameter of 100 nm. Their nucleation were more likely to occur at the edge area of Cu_2O layer I as shown in **Fig. 8 (c)**, which acted as defect site rather than the surface. It has also been reported that defect locations such as grain boundaries [22] and edge of a pit [23] are preferential nucleating sites for oxide island formation. Cu_2O grains later grew and coalesced together, which led to thickening of the oxide layer, replacement of Cu_2O layer I by many crossed and overlapping Cu_2O grains and formation of a new multiple Cu_2O layer termed Cu_2O layer II as shown in **Fig. 8 (d), (h), (k)** and **(l)**. The interface structure between Cu particle and disc shows a similar oxidation trend with time as shown in **Fig. 8 (e-h)** and the Cu disc surface was also oxidized after sintering. The thickness of oxide film increased

from 100 nm at 20 min bonding time to 450 nm at 240 min bonding time as shown in **Fig. 8 (i-l)**, which indicates that more Cu will be oxidized into Cu_2O with increasing time.

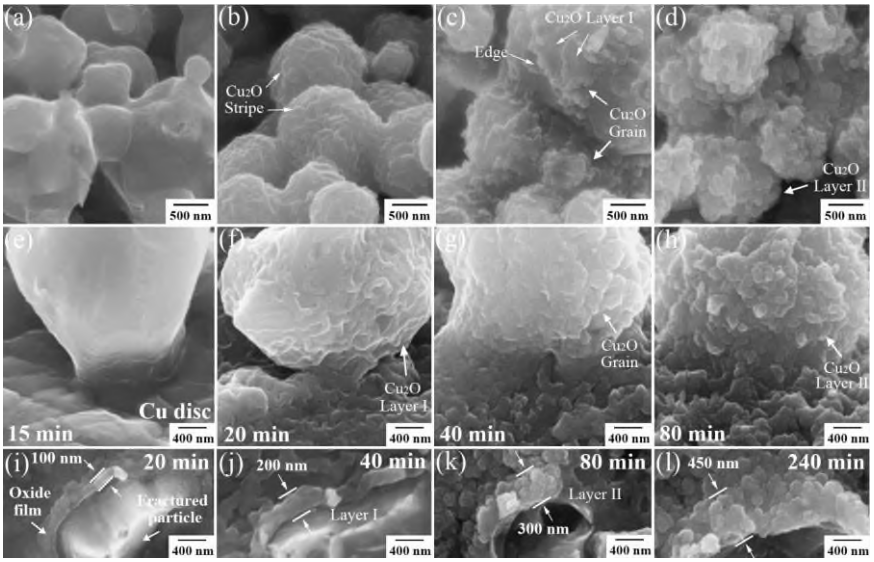

Fig. 8 SEM images of interfaces between Cu particles and between Cu particle and disc for 15 min (a, e), 20 min (b, f), 40 min (c, g) and 80 min (d, h). Comparison of oxide thickness between 20 min (i), 40 min (j), 80 min (k) and 240 min (l).

4.2 Variation in shear strength and fracture mechanism of joint

The bonding strength of Cu-Cu joints produced by sintering Cu is strongly related to contact area between sintering layer and substrate, and also the density of the sintered structure which is directly proportional to contact area between particles [24]. Made et al. [25] also proved that contact area was directly proportional to shear strength of the Cu–Cu thermal compression bond based on simulated and experimental results. After the pressure-assisted placement step, the joint was held at 220 °C with no pressure. Further increase of contact areas between Cu particle and disc and between Cu particles, results from relatively slow thermal diffusion. As discussed in Section 3, Cu particles are not found to have deformed significantly and their mean size almost unchanged even after sintering for 15 min at 220 °C. Zuo et al. [17] found a significant deformation of Cu nanoparticles

after sintering at 250 °C while Cu microparticles deformed little. The deformation of a dimple-like morphology which represents the further deformed and fully sintered Cu nanoparticles was also introduced by Yamakawa et al. [4] in the joint bonded at 350 °C with 15 MPa applied pressure. Zhong et al. [1] studied the consolidation behavior of Cu_6Sn_5 nanoparticles and found the sintering procedure is accompanied by increase in mean particle size and dramatic coalescence between particles with the particles eventually evolving into an integrated sphere. **Fig. 8** indicates that the sintering of reduced Cu particles was in the initial stage – formation of the sintering neck. Here, matter transport from the grain boundary between particles to the sintering neck dominates. Since matter transport from the bulk of the grain and the outer surface require higher temperature and pressure to activate, the matter transport from the grain boundary to the neck was assumed to be the main diffusion path to simplify the modeling of diffusion process. If the contact area is assumed to be a circular area with radius of x, the growing rate of contact area can be expressed as [26]:

$$\frac{x}{r}=\left(\frac{40\gamma a^3 D}{kT}\right)^{1/5} r^{-3/5}t^{1/5} \tag{1}$$

Where γ and r are surface free energy and radius of particle, respectively. a^3 is the volume of a diffusing vacancy, D is self-diffusion coefficient of Cu atom (note that Cu atom may have different D in the interface between Cu particle and disc and between Cu particles), k is Boltzmann's constant and T is temperature. The total contact area can be given by:

$$S=N\pi\left(\frac{40\gamma a^3 D}{kT}\times r^2 t\right)^{2/5} \tag{2}$$

Where N is total number of contacts between particles. Based on the above discussion, the contact area can be assumed to be proportional to the shear strength with a factor K on the premise of

non-oxidation, given as:

$$F = KBt^{2/5}, B = N\pi\left(\frac{40\gamma a^3 Dr^2}{kT}\right)^{2/5} \quad (3)$$

$$\log(F) = \log(KB) + \frac{2}{5}\log(t) \quad (4)$$

Where F is the shear strength. The shear strength results of joints bonded for 5 min, 7.5 min, 10 min, 12.5 min and 15 min are plotted as a function of bonding time, and compared with the model results based on Eq. (4) with the intercept fitted to the data to verify the slope as shown in **Fig. 9**. It is clear that the slope of the experimental results and the model prediction match very well. The above results indicate that the shear strength of joint by sintering Cu particle should increase with bonding time without the formation of Cu oxide structure as it will hinder the diffusion of metal atoms, which is in good agreement with shear test results.

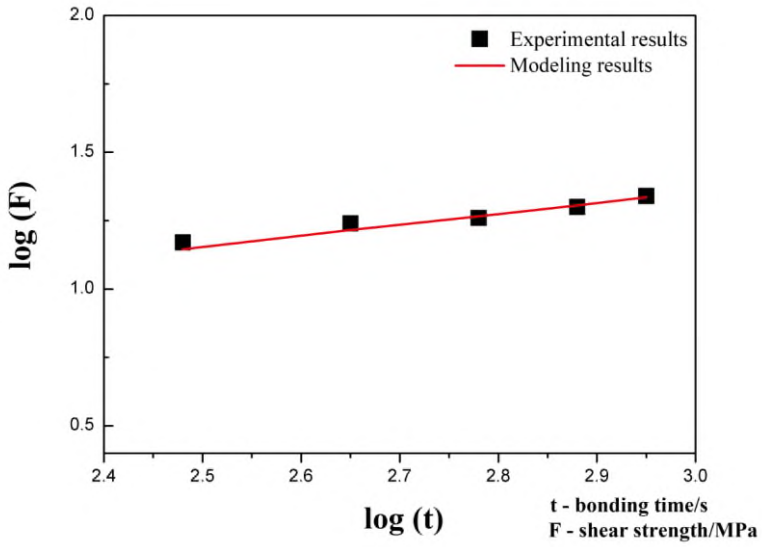

Fig. 9 Experimental results for Cu-Cu joint shear strength, compared with model predictions.

However, the shear strength of joints stops increasing with bonding time and eventually decreases when the oxide forms as discussed Section 3. In order to investigate the reason, the micro-fracture mode of sintered Cu particles bonded for 80 min was observed by SEM as shown in **Fig. 10**. The

submillimeter scale fracture surface of the joint (presented in Section 3) indicates that the Cu particles have deformed little after shearing and the fracture is mainly located at the interface between sintered Cu particles. However, the submicron scale fracture shows the evidence of plastic deformation of some Cu particles and fracture occurred inside Cu particles. These results indicates that there are three different fracture modes of the joint: 1) Brittle fracture at the interface between Cu particle and disc as shown in **Fig. 10 (a)**. 2) Brittle fracture at the interface between Cu particles as shown in **Fig. 10 (c)**. 3) Ductile fracture inside Cu particles with different deformation degrees as shown in **Fig. 10 (b) and (d)**. However, the Cu_2O film shows little plastic deformation in either case which indicates it is a brittle structure with poor strength, and there was a badpoor bonding between Cu core and Cu_2O film. Yuan et al. [27] has also reported that there was an obvious crack between the Cu_2O layer and Cu disc surface. It can be inferred that Cu_2O film was not able to provide effective strength for the whole bonding structure. In summary, formation of brittle Cu_2O structure with bad bonding to Cu core and disc and decrease of Cu-Cu contact area result in decreasing shear strength.

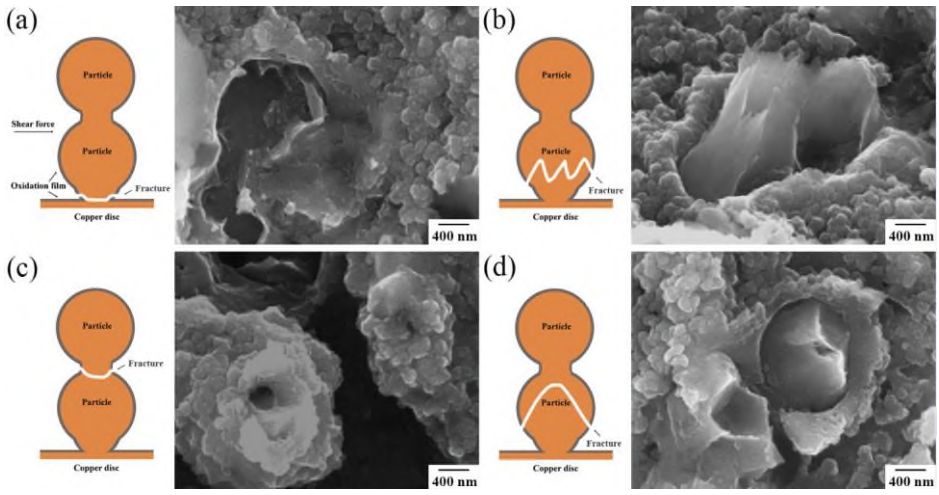

Fig. 10 SEM images of fractures between Cu particle and disc (a, b), and between Cu particles (c, d),

and corresponding schematic illustration of fracture mode.

5. Conclusions

In summary, in situ reduction-sintering of CuO nanoparticles by glycerol was proposed to fabricate strong Cu-Cu bonding for power electronics and the formation of oxide was depressed by the rapid sintering speed. The main results are given as follows:

(1) The best shear strength of 22 MPa for the joint was achieved by 15 min pressureless bonding at 220 °C in air which resulted in no Cu oxide structure. The shear strength of joint without oxide shows good agreement with the modeling results based on contact area theory.

(2) The only oxide that formed during bonding was Cu_2O, which shows morphological evolution from a laminar layer structure formed by growth and coalescence of Cu_2O nano-stripes to a multiple layer structure formed by crossed and overlapping Cu_2O nano-grains.

(3) Brittle fracture at the interface between Cu particles and between Cu particles and disc dominated while ductile fracture inside Cu particles was also found. The Cu_2O layer was a brittle structure with poor bonding to Cu core and disc, and its formation led to decreasing Cu-Cu contact area and joint shear strength.

Acknowledgement

The authors are grateful for the support from China Scholarship Council (CSC) 201806050001. The X-ray diffraction measurements were performed in Department of Chemistry, University of London.

References

[1] Y. Zhong, R. An, C. Wang, Z. Zheng, Z. Q. Liu, C. H. Liu, C. F. Li, T. K. Kim, S. Jin, Low Temperature Sintering Cu6Sn5 Nanoparticles for Superplastic and Super-uniform High Temperature

Circuit Interconnections. Small, 11 (2015), pp. 4097-4103.

[2] K. Kiełbasiński, J. Szałapak, M. Jakubowska, A. Młożniak, E. Zwierkowska, J. Krzemiński, M. Teodorczyk, Influence of nanoparticles content in silver paste on mechanical and electrical properties of LTJT joints, Adv. Powder. Technol., 26 (2015), pp. 907-913.

[3] A. Zinn, R. Stoltenberg, A. Fried, J. Chang, A. Elhawary, J. Beddow, F. Chiu, NanoCopper Based Solder-free Electronic Assembly, Nanotech, 2 (2012), pp. 71-74.

[4] T. Yamakawa, T. Takemoto, M. Shimoda, H. Nishikawa, K. Shiokawa, N. Terada, Influence of Joining Conditions on Bonding Strength of Joints: Efficacy of Low-Temperature Bonding Using Cu Nanoparticle Paste, J. Electron. Mater., 42 (2013), pp. 1260-1267.

[5] T. Fujimoto, T. Ogura, T. Sano, M. Takahashi, A. Hirose, Joining of Pure Copper Using Cu Nanoparticles Derived from CuO Paste, Mater. Trans., 56 (2015), pp. 992-996.

[6] J. Kwon, H. Cho, H. Eom, H. Lee, Y.D. Suh, H. Moon, J. Shin, S. Hong, S.H. Ko, Low-Temperature Oxidation-Free Selective Laser Sintering of Cu Nanoparticle Paste on a Polymer Substrate for the Flexible Touch Panel Applications, ACS Appl. Mater. Inter., 18 (2016), pp. 11575-82.

[7] Y. Zuo, J. Shen, Y. Hu, R. Gao, Improvement of oxidation resistance and bonding strength of Cu nanoparticles solder joints of Cu–Cu bonding by phosphating the nanoparticle, J. Mater. Process. Technol., 253 (2018), pp. 27-33.

[8] X. Liu and H. Nishikawa, Low-pressure Cu-Cu bonding using in-situ surface-modified microscale Cu particles for power device packaging, Scr. Mater., 120 (2016), pp. 80-84.

[9] R. Gao, S. He, Y.-A. Shen, H. Nishikawa, Effect of Substrates on Fracture Mechanism and

Process Optimization of Oxidation-Reduction Bonding with Copper Microparticles, J. Electron. Mater., 48 (2019), pp. 2263-2271.

[10] T. Ogura, T. Yagishita, S. Takata, T. Fujimoto, A. Hirose, Bondability of Copper Joints Formed Using a Mixed Paste of Ag2O and CuO for Low-Temperature Sinter Bonding, Mater. Trans., 54 (2013), pp. 860-865.

[11] Y. Gao, W. Li, C. Chen, H. Zhang, J. Jiu, C.F. Li, S. Nagao, K. Suganuma, Novel copper particle paste with self-reduction and self-protection characteristics for die attachment of power semiconductor under a nitrogen atmosphere. Mater Design 160 (2018), pp. 1265-1272.

[12] P. Guo, Y. Gao, Coalescence of Au Nanoparticles without Ligand Detachment, Phys. Rev. Lett., 124 (2020), pp. 066101.

[13] J.C. Love, L.A. Estroff, J.K. Kriebel, R.G. Nuzzo, G.M. Whitesides, Self-Assembled Monolayers of Thiolates on Metals as a Form of Nanotechnology, Chem. Rev. 105 (2005), pp. 1103-1169

[14] P. N. Amaniampong, Q. T. Trinh, J. J. Varghese, R. Behling, S. Valange, S. H. Mushrif, F. Jérôme, Unraveling the mechanism of the oxidation of glycerol to dicarboxylic acids over a sonochemically synthesized copper oxide catalyst, Green. Chem., 20 (2018), pp. 2730-2741.

[15] J.B. Chen, Q.H. Li, Y.H. Li, Z.Y. Liu, Z.H. Liu, Preparation of ultra-fine silver powders by precipitation-transformation method using glycerol as reductant, Mater. Sci. Eng. Powder. Metall., 18 (2013), pp. 874-881.

[16] Q. Yang, Z. Guo, X. Zhou, J. Zou, S. Liang, Ultrathin CuO nanowires grown by thermal oxidation of copper powders in air, Mater. Lett., 153 (2015), pp. 128-131.

[17] Y. Zuo, J. Shen, J. Xie and L. Xiang, Influence of Cu micro/nano-particles mixture and surface roughness on the shear strength of Cu-Cu joints, J. Mater. Process. Technol., 257 (2018), pp. 250-256.

[18] M. Lee, A.J.H. McGaughey, Energetics and kinetics of thec(2×2) to (2√2×√2)R45° transition during the early stages of Cu(100) oxidation, Phys. Rev. B., 83 (2011).

[19] P.A. Mulheran, J.A. Blackman, The origins of island size scaling in heterogeneous film growth, Phil. Mag. Lett., 72 (1995), pp. 55-60.

[20] C. Gattinoni, A. Michaelides, Atomistic details of oxide surfaces and surface oxidation: the example of copper and its oxides, Surf. Sci. Rep., 70 (2015), pp. 424-447.

[21] L.I. Hung, C.K. Tsung, W. Huang, P. Yang, Room-temperature formation of hollow Cu2O nanoparticles, Adv. Mater., 22 (2010), pp. 1910-4.

[22] G. Zhou, L. Wang, J.C. Yang, Effects of surface topology on the formation of oxide islands on Cu surfaces, J. Appl. Phys., 97 (2005), pp. 063509.

[23] J.C. Yang, M. Yeadon, B. Kolasa, J.M. Gibson, The Limited Role of Surface Defects as Nucleation Sites for. J. Electrochem. Soc., 146 (1999), pp. 2103-2106.

[24] Y. Zuo, J. Shen, H. Xu, R. Gao, Effect of different sizes of Cu nanoparticles on the shear strength of Cu-Cu joints, Mater. Lett., 199 (2017), pp. 13-16.

[25] R.I. Made, C.L. Gan, L. Yan, K.H.B. Kor, H.L. Chia, K.L. Pey, C.V. Thompson, Experimental characterization and modeling of the mechanical properties of Cu-Cu thermocompression bonds for three-dimensional integrated circuits, Acta Mater., 60 (2012), pp. 578-587.

[26] C.B. Carter, M.G. Norton, Ceramic Materials: Science and Engineering, Springer, New York,

2013.

[27] L. Yuan, Y. Wang, R. Mema, G. Zhou, Driving force and growth mechanism for spontaneous oxide nanowire formation during the thermal oxidation of metals, Acta Mater., 59 (2011), pp. 2491-2500.